Journal of Polyphenols
2024, 6 (4): 165–175
journal homepage: http://jpolyph.syphu.edu.cn

Exploration of potential mechanisms for the treatment of ulcerative colitis by *Solanum diphyllum* L. based on network pharmacology and molecular docking

Kexin Huang, Nan Yang, Bingxin Zhang, Ziqi Sun, Xiaoshu Zhang *

Faculty of Functional Food and Wine, Shenyang Pharmaceutical University, Shenyang 110016, China

Abstract Evidence of the advantages of *Solanum nigrum* L. for the treatment of ulcerative colitis is accumulating. However, research revealing the treatment of *Solanum diphyllum* L. against ulcerative colitis is scarce. In this study, the chemical components of the extract of *Solanum diphyllum* L. were characterized by LC-MS/MS, identifying 31 compounds by positive and negative total ion flow maps. A total of 425 component target genes and 1 900 disease target genes were obtained, and 121 intersection targets and 6 core targets were obtained after the intersection of the two genes by means of network pharmacology. GO analysis and KEGG analysis respectively obtained 20 signaling pathways such as anti-inflammation. The results of molecular docking showed that the chemical components could successfully dock with the target proteins of the disease such as SRC, EGFR, PTGS2, MMP9, HSP90AA1, ESR1. This study provided a scientific basis for the development and application of *Solanum diphyllum* L.

Keywords: LC-MS/MS; ulcerative colitis; *Solanum diphyllum* L.; network pharmacology; molecular docking

1 Introduction

Ulcerative colitis (UC) is a type of inflammatory bowel disease (IBD), a chronic and idiopathic inflammatory disease of the colonic mucosa [1], with a high prevalence of lesions confined to the mucosa and submucosa of the large intestine. The etiology and pathogenesis of ulcerative colitis is multifactorial and not fully understood. It includes genetic susceptibility, immune dysregulation, intestinal flora dysbiosis, epithelial barrier dysfunction, and many underlying environmental factors, which together result in persistent chronic inflammation [2].

Solanum diphyllum L. (SDL) is a variety of *Solanum nigrum* L., a plant of the genus *Solanum*. Because of its high medicinal and economic value, SDL is also regarded as a wild plant of great exploitation value. It is biologically adaptable and is currently used in clinical practice, and the whole plant can be used as medicine, which has the effect of dispersing blood stasis and eliminating swelling, clearing heat and removing toxins [3].

Phenolic-rich plants and their extracts, as well as individual phenolic compounds, have been shown to modulate the gut microbiota and gut barrier function [4]. However, the effects of phenolic compounds in *Solanum nigrum* L. on intestinal health have not received sufficient attention, especially for the

* Corresponding author: Xiaoshu Zhang (xiaoshu2397@163.com).
These authors have no conflict of interest to declare.

therapeutic potential of SDL in UC has not been investigated so far.

Therefore, through Swiss Target Prediction, OMIM and GeneCards databases, this study constructed a regulatory network of components and targets and a Protein-protein interaction network, and screened out the action pathway of SDL in the treatment of UC, and conducted molecular docking to provide scientific basis for further exploring the mechanism of action of SDL in the treatment of UC.

2 Materials and methods

2.1 Chemicals and reagents

SDL was harvested in the suburbs of Shenyang, Liaoning Province, China. The fruits were extracted with pure water (1:10, g/mL) at 50 °C for 50 min, and then the solution was extracted with 200 mL 50% ethanol. The resulting ethanol extract was filtered through filter paper and concentrated by rotary evaporation at 40 °C until dryness.

2.2 Determination of total phenol content (TPC)

The polyphenol content was determined by Folin-ciocalteu spectrophotometric method, based on the method of Rumpf, et al. [5] with modifications. Briefly, gallic acid standard samples (0 mg/mL, 12.5 mg/mL, 25 mg/mL, 50 mg/mL, 100 mg/mL, 200 mg/mL) and extracts (2 mg/mL) were prepared, and then added 0.5 mL FC, 1.5 mL 20% Na_2CO_3, and a water bath of 50 °C for 30 min. The absorbance of the supernatant was measured at 765 nm using a microplate reader. The standard curve was plotted with gallic acid concentration as the horizontal and vertical scales and absorbance value as the vertical coordinate. After linear regression, the equation of gallic acid concentration versus absorbance value was obtained as: $y = 0.634\ 6x - 0.683\ 9$, $R^2 = 0.994\ 9$.

Then the amount of polyphenols extracted from SDL was calculated according to Equation (1) and expressed as the mass of gallic acid mg per gram of SDL.

The polyphenol content of SDL=

$$\frac{C \times V \times N}{M} \times 100\% \quad (1)$$

C is the polyphenol concentration (mg/mL); V is the volume of extract (mL); N is the number of dilutions; M is the sample mass (g).

2.3 LC-MS/MS analysis

The total extracts of SDL were analyzed by full scanning under positive and negative ion modes. Parameters for liquid chromatography: Agilent 1260 HPLC system equipped with Agilent ZORBAX bsC18 column, column temperature set at 30 ℃. The temperature of the automatic sampler was set at 4 ℃, the sample volume was set at 1 μL, and the flow rate was set at 1 mL/min. The mobile phase consisted of 0.1% phosphoric water and methanol. Gradient conditions: 0−5 min, 2% methanol; 5−10 min, 2%−5% methanol; 10−40 min, 5%−45% methanol; 40−60 min, 45% methanol.

Parameters used for mass spectrum: Agilent 6530 QTOF/MS mass spectrometer, positive and negative ion modes using electrospray ionization (ESI). The MS scanning range is set to 100−500 Da, and the MS/MS scanning range is set to 50−500 Da. The capillary voltage was set at 3.5 kV, the dry gas flow was set at 9 mL/min, and the temperature was set at 350 ℃. The atomizer gas pressure is set at 45 psi. Sheath gas flow and temperature were maintained at 12 mL/min and 400 ℃, respectively. Nitrogen is used as an auxiliary gas as well as an atomizing gas. The fragmentation voltage and collision energy (CE) were set at 150 V and 40 V, respectively. Agilent MassHunter workstation was used for data acquisition (version B.05.01). Data were processed using Agilent MassHunter qualitative analysis (version B.06.00).

2.4 Active ingredient screening and target prediction

The LC-MS/MS analyzed components of the extracts of SDL were searched in the PubChem (https://pubchem.ncbi.nlm.nih.gov/) database, and the corresponding Isomeric SMILES numbers were queried according to the names of the components,

which were imported into Swiss ADME (http://www.swissadme.ch), and one "High" and two "Yes" were set as the screening conditions to select the active components; Then the active ingredients were imported into the Swiss Target Prediction (http://swisstargetprediction.ch/) database, and the species was limited to "Homo sapiens", and the official gene name of the target was obtained, and the preliminary screening condition was set as "Probability > 0"; the compound-target network diagram was constructed by using Cytoscape 3.9.0 software.

2.5 Disease-related target prediction

Using "Ulcer Colitis" as the keyword, GeneCards (https://www.genecards.org/) and OMIM (https://www.omim.org/) were used to screen for related targets, and the two disease databases were merged. The target information of the two disease databases was combined, and the Venn diagram was plotted using Venny 2.1.0 (https://bioinfogp.cnb.csic.es/tools/venny/).

2.6 Construction of protein interaction networks

Disease drug critical genes were accessed through Venn diagram online tool. Cytoscape 3.9.0 software was used to create the active ingredient target network map, and with the help of String (https://cn.string-db.org/) database, the species was set as "Homo sapiens", and the default minimum interactions score was 0.4, to get the protein-protein interaction (PPI) network map.

2.7 Gene ontology and KEGG analyses

The common targets were analyzed using the David database (http://www.david.ncifcrf.gov) and visualized using the online mapping platform Microbiology (http://www.bioinformatics.com.cn/).

2.8 Key active ingredient prediction

Cytoscape 3.9.0 software was used to predict the key active ingredients.

2.9 Molecular docking

Search for protein structure from PDB data (https://www.rcsb.org/), download 3D structure *PDB Format of SRC, EGFR, PTGS2, MMP9, HSP90AA1, ESR1, modify the structure of protein and compound with Discovery Studio 2016 Client software.

3 Results

3.1 Total phenolic content of SDL extract

Based on the standard curve: $y = 0.634\ 6x - 0.683\ 9$, we calculated the total phenol content in SDL extract as 8.55 mg/g.

3.2 LC-MS/MS analysis of SDL extract

LC-MS/MS analysis of SDL extract initially identified 31 compounds, 29 of which were identified by positive ion mode. There are 2 phenolic compounds, including chlorogenic acid and caffeic acid. According to molecular weight, retention time (t_R), fragment ions, chemical class and name of each compound (Table 1 and Table 2), their identities were finally determined. The LC-MS/MS positive and negative ion chromatogram of SDL was shown in Fig. 1 and Fig. 2.

3.3 Active ingredient screening and target prediction

There is an 18-constituent from SDL that includes γ-aminobutyric acid, nicotinicacid, proline, valine, adenine, solamargine, solasonine, L-valinol, 7-aminoheptanoic acid, 2(R)-hydroxy-2-methylbutyronitrile-β-D-glucopyranoside, 3-hydroxyglutarica-cid, 4-Acetamidobutyricacid, 2(6-Isocyanatohexylaminocarbon-ylamino)-6-methyl-4[1h]pyrimidinone, N-[2-chloro-5-(3,6-d-ihydro-2H-pyran-4-yl)p-yridin-3-yl]methan-esulfonamide, 3-methylsulfanyl-5-[(3-methylsulfanyl-5-[(3-methylsulfanyl-1H-1,2,4-triazol-5-yl)methyl]-1H-1,2,4-

triazole, 2-(3-phenylpropyl)pyridine, 2-cyclohexyl1-benzothiophene, and safrole. In order to better demonstrate the intricate relationship between active ingredients and targets, Cytoscape 3.9.0 software was used to construct a compound-target network graph containing 551 nodes and 743 edges (Fig. 3).

Table 1 Compounds identified in SDL extract by LC-MS/MS at positive ion mode

No.	t_R/min	Precursor Ion $[M+H]^+$ (m/z)	Theoretical mass (m/z)	Elemental composition	Name of the compound
1	1.549	104.107 6	104.160 0	$C_5H_{13}NO$	L-Valinol
2	1.587	247.057 8	247.057 9	$C_9H_6N_6O_3$	1,3,5-Triazine, 2,4,6-tris(cyanomethoxy)-
3	1.674	146.117 0	146.201 0	$C_7H_{15}NO_2$	7-Aminoheptanoic acid
4	1.697	104.103 2	104.127 1	$C_4H_9NO_2$	γ-Aminobutyric acid
5	1.814	116.070 1	116.071 2	$C_5H_9NO_2$	Poline
6	1.932	124.038 9	124.039 9	$C_6H_5NO_2$	Nicotinic acid
7	1.957	262.129 2	262.269 1	$C_{11}H_{19}NO_6$	2(R)-Hydroxy-2-methylbutyronitrile-β-D-glucopyranoside
8	1.975	280.138 8	280.132 1	$C_{11}H_{21}N0_7$	N-(1-Deoxy-1-fructosyl)valine
9	2.050	118.086 6	118.086 8	$C_5H_{11}NO_2$	Valine
10	2.424	215.014 5	215.014 0	$C_4H_{10}N_2O_4S_2$	Hydroxymethanesulfinic acid
11	2.875	136.061 9	136.062 3	$C_5H_5N_5$	Adenine
12	3.942	149.044 4	149.110 9	$C_5H_8O_5$	3-Hydroxyglutaric acid
13	3.942	146.080 6	146.081 1	$C_6H_{11}NO_3$	4-Acetamidobutyric acid
14	5.552	294.155 0	294.321 7	$C_{13}H_{19}N_5O_3$	2(6-Isocyanatohexylaminocarbonylamino)-6-methyl-4[1h]pyrimidinone
15	24.258	289.741 1	289.753 2	$C_{11}H_{13}ClN_2O_3S$	N-[2-Chloro-5-(3,6-dihydro-2H-pyran-4-yl) pyridin-3-yl]methanesulfonamide
16	24.258	243.347 9	243.310 4	$C_7H_{10}N_6S_2$	3-Methylsulfanyl-5-[(3-methylsulfanyl-1H-1,2,4-triazol-5-yl)methyl]-1H-1,2,4-triazole
17	28.403	355.102 2	355.087 4	$C_{16}H_{18}O_9$	Chlorogenic acid
18	30.188	423.093 6	423.093 2	$C_{20}H_{14}N_4O_7$	5-Ethyl-5-(4-nitro-1,3-dioxoisoindol-2-yl)-1-phenyl-1,3-diazinane-2,4,6-trione
19	31.589	463.085 4	463.088 9	$C_{17}H_{14}N_6O_{10}$	2-(2-Aminoethylamino)-1,3-bis(3,5-dinitrophenyl)propane-1,3-dione
20	32.106	458.129 8	458.130 1	$C_{19}H_{23}NO_{12}$	1-[(2R,3R,4R)-3,4-diacetyloxy-5-[[(2S)-3-carboxy-2-hydroxypropanoyl]oxymethyl] oxolan-2-yl]-4H-pyridine-3-carboxylic acid
21	32.440	409.183 9	409.184 4	$C_{18}H_{20}N_{10}O_2$	6-(Azetidin-1-yl)-N-[1-methyl-5-(methylcarbamoyl)pyrazol-4-yl]-3-(pyrimidin-5-ylamino)pyrazine-2-carboxamide

(to be continued)

Continued Table 1

No.	t_R/min	Precursor Ion $[M+H]^+$ (*m*/*z*)	Theoretical mass (*m*/*z*)	Elemental composition	Name of the compound
22	33,024	517.226 5	517.221 7	$C_{21}H_{28}N_{10}O_6$	Benzyl N-[(1R)-1-[(2S,6R)-5-azido-6-[(1R,2R,3S)-4,6-diazido-2,3-dihydroxycyclohexyl]oxyoxan-2-yl]ethyl] carbamate
23	33.357	198.127 9	198.271 5	$C_{14}H_{15}N$	2-(3-Phenylpropyl)pyridine
24	33.791	579.226 2	579.226 5	$C_{21}H_{34}N_6O_{13}$	H-Asp-Asn-Glu-Thr-Thr-OH
25	38.995	663.155 0	663.148 8	$C_{30}H_{30}O_{17}$	(Z)-2,3-Dihydroxybut-2-enedioic acid
26	40.476	884.503 3	884.500 8	$C_{45}H_{73}NO_{16}$	Solasonine or Isomer
27	45.073	868.506 2	868.505 8	$C_{45}H_{73}NO_{15}$	Solamargine
28	49.729	217.104 1	217.341 6	$C_{14}H_{16}S$	2-Cyclohexyl-1-benzothiophene
29	49.729	163.074 5	163.180 8	$C_{10}H_{10}O_2$	Safrole

Table 2 Compounds identifi ed in SDL extract by LC-MS/MS at negative ion mode

No.	t_R/min	Precursor Ion $[M+H]^-$ (*m*/*z*)	Theoretical mass (*m*/*z*)	Elemental composition	Name of the compound
1	2.053	179.034 8	179.034 1	$C_9H_8O_4$	Caffeic acid
2	36.589	625.139 6	625.139 9	$C_{27}H_{30}O_{17}$	6-Hydroxyluteolin

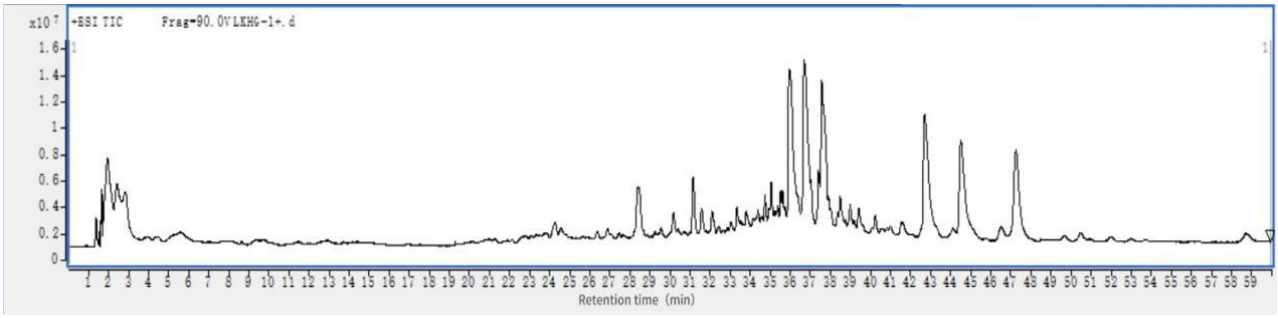

Fig. 1 Total ion chromatogram of positive ion LC-MS/MS of SDL extract

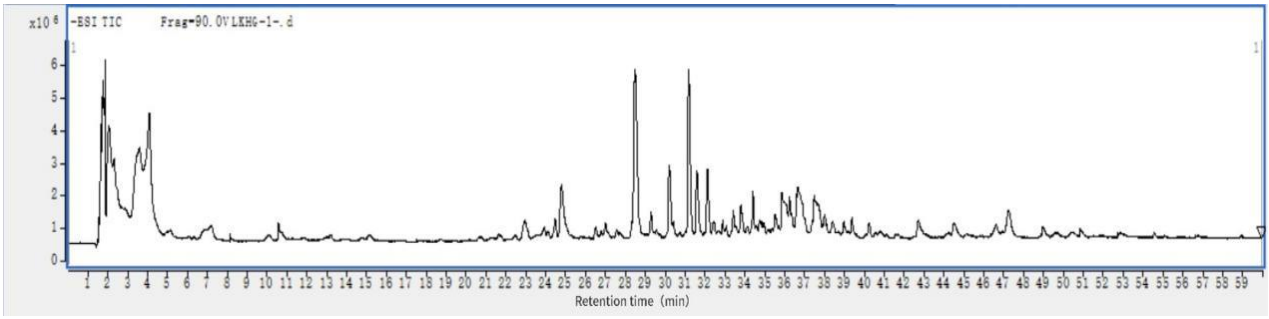

Fig. 2 Total ion chromatogram of negative ion LC-MS/MS of SDL extract

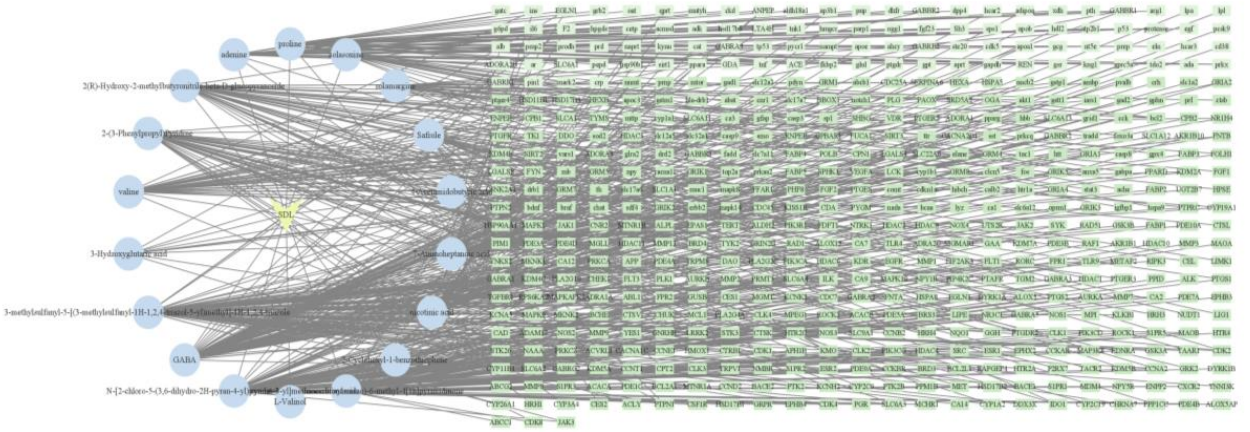

Fig. 3 "Compounds-targets" network

3.4 Disease target prediction results

The target targets were screened by GeneCards and OMIM databases, and a total of 2 021 colitis disease targets were obtained after deleting duplicates. By importing the Venn diagram of Venny 2.1.0 online tool together with 546 active ingredient targets for comparison, 121 core gene targets were obtained (Fig. 4).

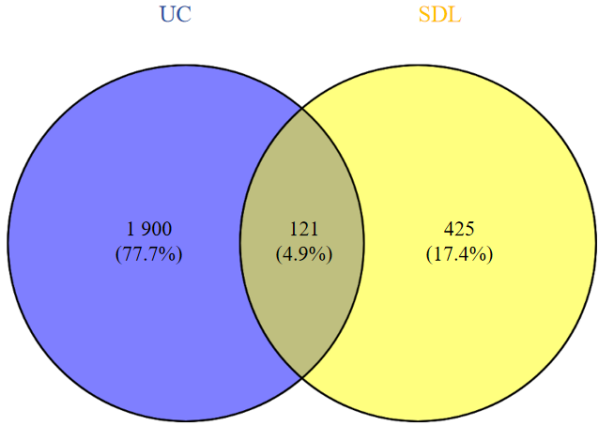

Fig. 4 "Disease-component" target Venn diagram

3.5 Construction of protein interaction network PPI results

The biological species was set as "Homo sapiens", and 121 core gene targets were selected through the veen diagram. The components and corresponding target information were imported into the String database to draw the interaction network, and the high confidence was selected as 0.400. The obtained core targets were saved and imported into Cytoscape 3.9.0 to draw the protein-protein interaction network of the core proteins, as shown in Fig. 5. The protein interaction information was obtained with 119 nodes and 1 225 edges. The larger the number of targets connected to each target and the larger the node area, the more important the target is in the PPI network.

3.6 GO function and enrichment analysis of KEGG pathway

GO functional analysis was performed on 121 key targets through the DAVID database, and a total of 710 GO entries were obtained, of which, 528 entries were covered for biological processes, including protein phosphorylation, signal transduction,

inflammatory response, negative regulation of apoptotic process, cell differentiation, etc.; 70 entries for cellular composition, including plasma membrane, cytoplasm, cytosol, nucleus, membrane, etc.; In terms of molecular function, there are 112 entries, including protein binding, ATP binding, protein serine/threonine/tyrosine kinase activity, identical protein binding, protein kinase activity. The results are shown in Fig. 6.

KEGG enrichment analysis yielded a total of 144 pathways involving Pathways in cancer, VEGF signaling pathway, PI3K-Akt signaling pathway, EGFR tyrosine kinase inhibitor resistance, Lipid and atherosclerosis, etc. We selected the top 10 GOs and the top 20 pathways with small P-values for visualization and analysis, and the results are shown in Fig. 7.

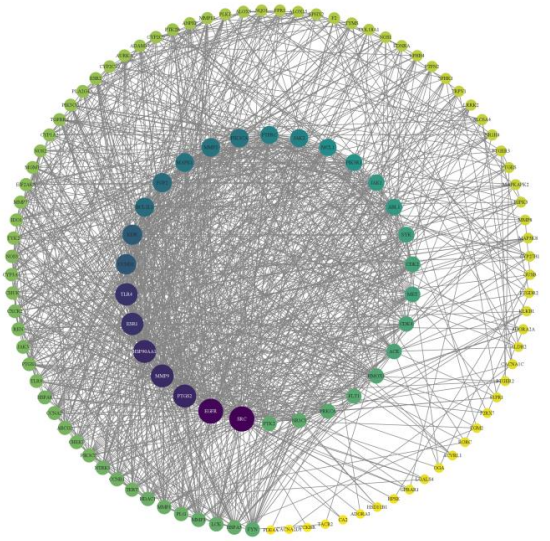

Fig. 5 Network of protein-protein interaction

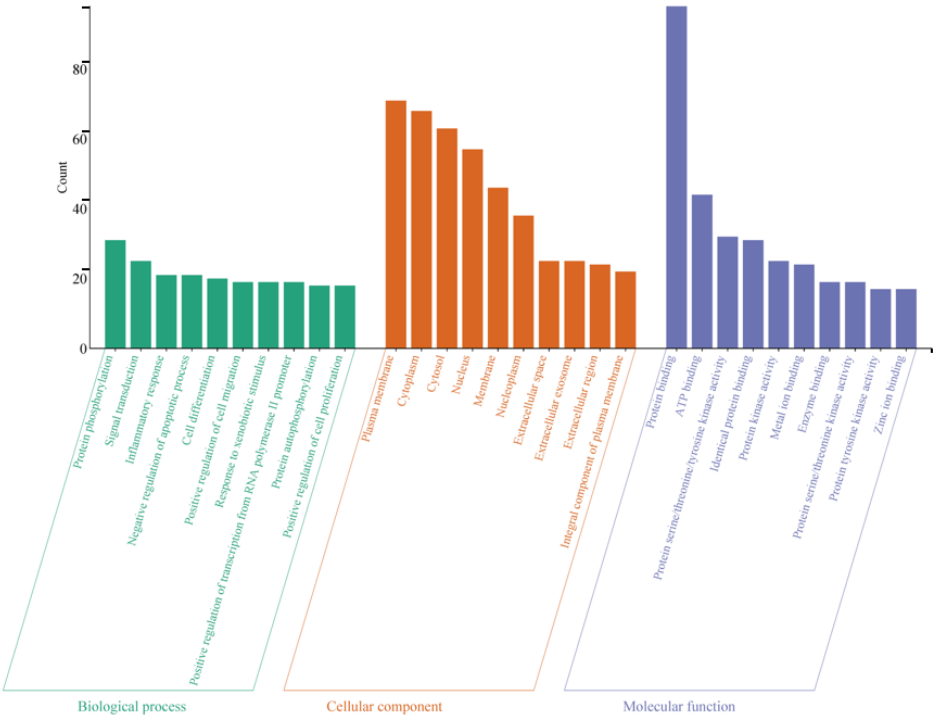

Fig. 6 GO functional enrichment analysis diagram

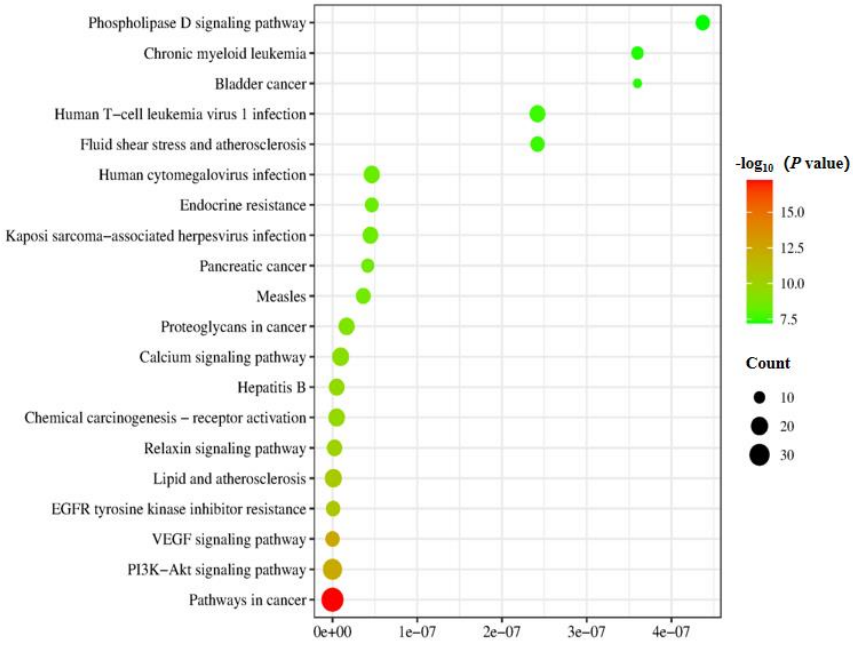

Fig. 7 KEGG pathway enrichment analysis

3.7 Key Active Ingredient prediction

The top ten compounds was selected in terms of degree values, listed in Table 3.

Table 3 Key Active Ingredients

Degree	Name
92.0	2(6-Isocyanatohexylaminocarbonylamino)-6-methyl-4[1h]pyrimidinone
90.0	N-[2-Chloro-5-(3,6-dihydro-2H-pyran-4-yl)pyridin-3-yl]methanesulfonamide
86.0	3-Methylsulfanyl-5-[(3-methylsulfanyl-1H-1,2,4-triazol-5-yl)methyl]-1H-1,2,4-triazole
52.0	7-Aminoheptanoic acid
46.0	Nicotinic acid
44.0	Proline
42.0	Valine
39.0	2-(3-Phenylpropyl)pyridine
39.0	2(R)-Hydroxy-2-methylbutyronitrile-*β*-D-glucopyranoside
31.0	Adenine

3.8 Molecular docking verification

Dicovery Stiudio 2016 was adopted The LibDock module of Client software analyzed 5 compounds with high chemical component content and key targets SRC (8bq3), EGFR (7u99), PTGS2 (5f19), MMP9 (5th6), HSP90AA1 (5njx), ESR1 (1x7r). Molecular docking verification was carried out, and the molecular docking scores of each ligand molecule and receptor protein were shown in Table 4. The docking scores were greater than 100, indicating that these compounds and proteins could dock well, further proving the reliability and effectiveness of SDL in the treatment of UC. The 2D and 3D maps clearly illustrate the binding pattern of the compound-protein docking results Fig. 8 and Fig. 9.

Table 4 Interaction between the active substance and the target protein

Entry	Protein	PDB ID	LibDock score	Interaction
2(6-Isocyanatohexylaminocarbonylamino)-6-methyl-4[1h] pyrimidinone	EGFR	7U99	105.129	Conventional hydrogen bond; Carbon hydrogen bond; Unfavorable positive-positive; Pi-anion
	ESR1	1X7R	106.455	Attractive charge; Conventional hydrogen bond; Carbon hydrogen bond; Pi-sigma; Pi-alky1
	MMP9	5TH6	132.568	Conventional hydrogen bond; Carbon hydrogen bond; Pi-alky1
2(*R*)-Hydroxy-2-methylbutyronitrile-*β*-D-glucopyranoside	ESR1	1X7R	101.311	Conventional hydrogen bond; Carbon hydrogen bond; Alky1
	MMP9	5TH6	120.275	Conventional hydrogen bond; Carbon hydrogen bond; Unfavorable acceptor acceptor; Alky1; Pi-alky1
3-Methylsulfanyl-5-[(3-methylsulfanyl-1H-1,2,4-triazol-5-yl)methyl]-1H-1,2,4-triazole	MMP9	5TH6	106.162	Conventional hydrogen bond; Carbon hydrogen bond; Pi-pi stacked; Alky1; Pi-alky1

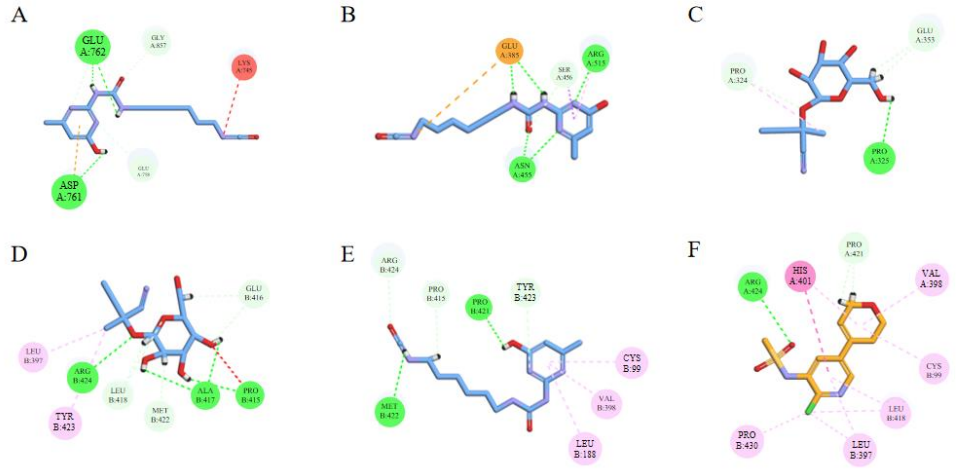

Fig. 8 2D model diagram of the docking between SDL components and target proteins

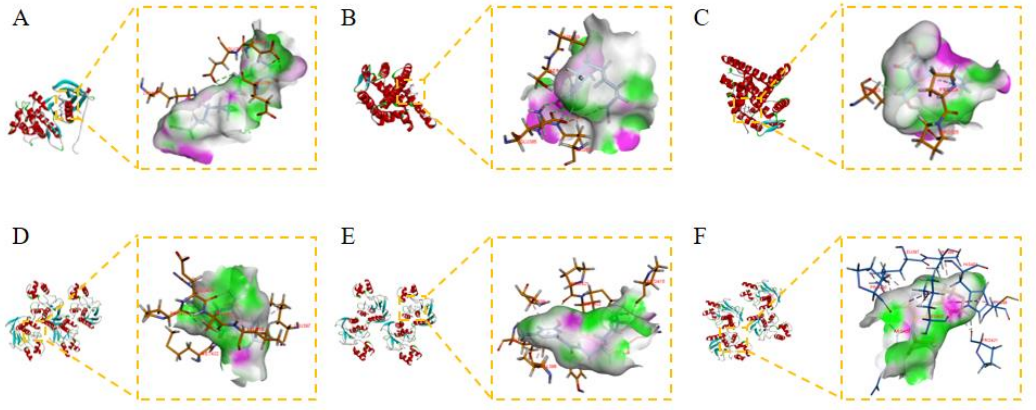

Fig. 9 SDL of molecular docking between key compounds and core target proteins

4 Discussion

The whole plant of SDL is used medicinally and contains a variety of anti-inflammatory and antioxidant active ingredients such as lobelia alkaloids and macadamia alkaloids, which are used in the treatment of various cancers [6].

31 compounds were identified by LC-MS/MS and analyzed the mechanism of the effects of SDL extract on UC by network pharmacology and molecular docking techniques. A total of 6 targets including SRC, EGFR, PTGS2, MMP9, HSP90AA1, ESR1 were selected for SDL treatment of UC. Among these proteins, MMP9 is closely implicated in both generation and persistence of inflammatory state in UC [7]. It was reported that Src is a member of the highly conserved non-receptor tyrosine kinases family involved in a variety of intracellular signal transduction [8]. The studies have reported that the activation of Src kinase not only has a harmful effect on the intestinal epithelial barrier, but also plays a crucial role in the inflammatory response mechanism of colitis [9, 10]. The inflammatory response triggered by LPS in macrophages is mediated by TLR4, and activation of TLR4 also triggers several protein tyrosine kinases, including Src, Syk, and SFK kinases [11]. Src is involved in LPS/TLR4 mediated inflammatory response [12]. EGFR signaling is a known mediator of colorectal carcinogenesis. It has proved to be an effective biomarker of UC or target for chemoprevention in patients with inflammatory bowel disease [13]. PTGS2, commonly known as cyclooxygenase-2 (COX-2), promotes angiogenesis by upregulating expression of vascular endothelial growth factor (VEGF) [14]. HSP90, a molecular chaperone with high conservation, is believed to act as a cancer promoter in the formation of different types of tumors, including CRC. HSP90AA1, a member of the HSP90 family that is responsive to stress, controls various proto-oncogene products and crucial signal transduction factors. According to recent research, HSP90AA1 has been found to facilitate the advancement of tumors, invasion, and resistance to chemotherapy. HSP90AA1, acting as an external element, can additionally facilitate the inflammatory reaction [15]. Estrogen is an essential sex factor, and ESR1 mainly encodes the nuclear hormone receptor. ESR1 shows the ability to suppress active inflammation and immune response [16], and estradiol can suppress psoriatic inflammation in mice by regulating neutrophil and macrophage functions [17].

GO analysis indicated that UC related biological processes were mainly protein phosphorylation, signal transduction, inflammatory response, negative regulation of apoptotic process, cell differentiation. KEGG pathways were further confirmed in present research, mainly including Pathways in cancer, VEGF signaling pathway, PI3K-Akt signaling pathway, EGFR tyrosine kinase inhibitor resistance, Lipid and atherosclerosis. The PI3K/Akt signaling pathway is associated with various biological processes, including cell cycle, apoptosis, metabolism and angiogenesis [18]. Suppression of the PI3K/Akt signaling pathway may help to regulate the balance of Tfh/Treg cells and reduce inflammatory response in experimental colitis [19]. VEGF is a key pro-angiogenic growth factor in UC pathogenesis. Unlike other pro-angiogenic growth factors, VEGF upregulation is harmful in UC healing and its inhibition is beneficial [20]. One study found for the first time that selective inhibition of VEGF signaling pathway might be a new, safe approach in UC treatment [21]. These results indicate that SDL can achieve therapeutic effect on UC through multi-component, multi-target and multi-pathway.

5 Conclusion

In summary, this study was conducted to identify the components of SDL by LC-MS/MS analysis to determine their key active compositions. Then, network pharmacology was utilized to elucidate the interactions among the key components, targets and pathways of SDL. The application of molecular docking technique further confirmed the binding activities between the core components and the key target proteins. This study visualized the specific mechanism of action of SDL for the treatment of UC, which may provide reference for further development

of SDL.

References

[1] Ordás I, Eckmann L, Talamini M, et al. Ulcerative colitis [J]. Lancet, 2023, 402 (10401): 571-584.

[2] Pituch-Zdanowska A, Dembiński Ł, Banaszkiewicz A. Old but fancy: Curcumin in ulcerative colitis-current overview [J]. Nutrients, 2022, 14 (24): 5249.

[3] Zhou J, Pan ZY, Zhao Y, et al. Physiological growth response of *Solanum mongolicum* seedlings to cadmium stress [J]. Plants of Guangxi, 2022, 42 (4): 628-638.

[4] Wan MLY, Co VA, El-Nezami H. Dietary polyphenol impact on gut health and microbiota [J]. Crit Rev Food Sci Nutr, 2021, 61 (4): 690-711.

[5] Rumpf J, Burger R, Schulze M. Statistical evaluation of DPPH, ABTS, FRAP, and Folin-Ciocalteu assays to assess the antioxidant capacity of lignins [J]. Int J Biol Macromol, 2023, 223: 123470.

[6] Ji YB, Wang SH, Gao SY, et al. Effect of solanine on sialic acid and sealing degree of tumor cell membrane in H22 tumor-bearing mice [J]. Chin Herb Med, 2005, 36 (1): 79.

[7] Marshall DC, Lyman SK, McCauley S, et al. Selective allosteric inhibition of MMP9 is efficacious in preclinical models of ulcerative colitis and colorectal cancer [J]. PLoS One, 2015, 10 (5): e0127063.

[8] Cho RL, Yang CC, Lee IT, et al. Lipopolysaccharide induces ICAM-1 expression via a c-Src/NADPH oxidase/ROS-dependent NF-κB pathway in human pulmonary alveolar epithelial cells [J]. Am J Physiol Lung Cell Mol Physiol, 2016, 310 (7): L639-L657.

[9] Chelakkot C, Ghim J, Rajasekaran N, et al. Intestinal epithelial cell-specific deletion of PLD2 alleviates DSS-induced colitis by regulating occludin [J]. Sci Rep, 2017, 7 (1): 1573.

[10] Kim HG, Kim MY, Cho JY. Alisma canaliculatum ethanol extract suppresses inflammatory responses in LPS-stimulated macrophages, HCl/EtOH-induced gastritis, and DSS-triggered colitis by targeting Src/Syk and TAK1 activities [J]. J Ethnopharmacol, 2018, 219: 202-212.

[11] Chiou WF, Don MJ, Liao JF, et al. Psoralidin inhibits LPS-induced iNOS expression via repressing Syk-mediated activation of PI3K-IKK-IκB signaling pathways [J]. Eur J Pharmacol, 2011, 650: 102-109.

[12] Byeon SE, Yi YS, Oh J, et al. The role of src kinase in macrophage-mediated inflammatory responses [J]. Mediat Inflamm, 2012, 2012: 512926.

[13] Hardbower DM, Coburn LA, Asim M, et al. EGFR-mediated macrophage activation promotes colitis-associated tumorigenesis [J]. Oncogene, 2017, 36 (27): 3807-3819.

[14] Manieri N, Mack M, Himmelrich M, et al. Stappenbeck mucosally transplanted mesenchymal stem cells stimulate intestinal healing by promoting angiogenesis [J]. J Clin Invest, 2015, 125 (9): 3606-3618.

[15] Grimstad T, Kvivik I, Kvaløy JT, et al. Heat shock protein 90 and inflammatory activity in newly onset Crohn's disease scand [J]. J Gastroenterol, 2018, 53 (12): 1453-1458.

[16] Li F, Boon ACM, Michelson AP, et al. Estrogen hormone is an essential sex factor inhibiting inflammation and immune response in COVID-19 [J]. Sci Rep, 2022, 12 (1): 9462.

[17] Adachi A, Honda T, Egawa G, et al. Estradiol suppresses psoriatic inflammation in mice by regulating neutrophil and macrophage functions [J]. J Allergy Clin Immunol, 2022, 150 (4): 909-919.

[18] Ashrafizadeh M, Zarrabi A, Hushmandi K, et al. Association of the epithelial-mesenchymal transition (EMT) with cisplatin resistance [J]. Int J Mol Sci, 2020, 21 (11): 4002.

[19] Jin J, Zhong Y, Long J, et al. Ginsenoside Rg1 relieves experimental colitis by regulating balanced differentiation of Tfh/Treg cells [J]. Int Immunopharmacol, 2021, 100: 108133.

[20] Tolstanova G, Khomenko T, Deng X, et al. Neutralizing anti-vascular endothelial growth factor (VEGF) antibody reduces severity of experimental ulcerative colitis in rats: Direct evidence for the pathogenic role of VEGF J. pharmacol [J]. Exp Ther, 2009, 328: 749-757.

[21] Tolstanova G, Khomenko T, Deng XM, et al. New molecular mechanisms of the unexpectedly complex role of VEGF in ulcerative colitis [J]. Biochem Biophys Res Commun, 2010, 399 (4): 613-616.